PAPER

Check for updates

Mannose-decorated polymersomes loaded with antigens and TLR7/8 agonists targeting antigen-presenting cells for enhancing vaccine efficacy†

Jong-Woo Lim, [ID] ‡[a] So-Eun Lee,‡[b] Hongjun Park,[b] Sojeong Lee,[b] Minjoo Yeom,[a] Seungjoo Haam [ID] *[b] and Daesub Song [ID] *[a]

Directing nanoparticles to specific receptors on antigen-presenting cells (APCs) is a promising strategy for inducing robust immune responses. This approach effectively enhances antigen (Ag) uptake, processing, and presentation, leading to improved Ag-specific immunogenicity. In this study, we introduce a novel method for targeting mannose-binding C-type lectin receptors (mannose receptor, CD206) using mannose-decorated nanoparticles to enhance vaccine efficacy. We developed mannose-decorated polymersomes (Man-PSomes) for co-delivering the model Ag-ovalbumin (OVA) within the inner core and the TLR7/8 dual agonist adjuvant resiquimod (R848) within the bilayer of the hydrophobic membrane. This nanoparticulate vaccine delivery system demonstrated the sustained release of Ag in cellular environments and efficiently facilitated the cellular uptake of Ag and R848 into APCs. Additionally, OVA and R848 co-encapsulated in Man-PSomes (OVA/R848/Man-PSomes) significantly increased the efficiency of APC maturation, cross-presentation, and pro-inflammatory cytokine secretion by T cells *in vitro* compared to that of soluble OVA/R848 or non-Man-PSomes. OVA/R848/Man-PSomes induced effective Ag-specific antibody production and T cell-mediated cytokine induction *in vivo*, suggesting that Man-PSomes encapsulating OVA and R848 could serve as potent nanoparticulate vaccine delivery systems that induce cellular and humoral immune responses.

Introduction

The coronavirus disease (COVID-19) pandemic emphasized the importance of developing effective vaccines. Inactivated, live-attenuated, and recombinant protein vaccines are the most widely used and approved vaccines for infectious diseases.[1,2] However, these conventional vaccines have several issues that must be addressed. Live-attenuated vaccines, while offering superior efficacy, may pose safety concerns because of the potential for secondary mutations. Although affordable and safe protein subunit vaccines can address these safety concerns, there may be limitations to eliciting robust immune responses.[3]

Nanoparticulated vaccine systems have been advocated to enhance the immunogenicity of vaccines and ensure safety.

Nanoparticles offer several advantages as vehicles, including improved antigen (Ag) protection, sustained payload release, and efficient cellular uptake.[4–6] Various nanoparticles are being used, including micelles, liposomes, polyplex, and dendrimers.[7–9] Of these, lipid nanoparticles were widely utilized as vaccine delivery vehicles in the COVID-19 era and are now commercially approved and officially available in many countries.[10–12] However, due to the monopolization of lipid-related patents by some companies, there is a need to explore novel lipids or alternatives such as biocompatible polymers. Furthermore, to enhance immune responses by nanoparticulate vaccine delivery systems, delivery technologies must specifically target antigen-presenting cells (APCs).

Targeted delivery of antigens to APCs is an effective strategy for eliciting robust Ag-specific immune responses.[13,14] APCs are a crucial link between the innate and adaptive immune systems, facilitating the induction of protective immunity. APCs such as macrophages and dendritic cells are rich in mannose receptors.[15] Mannose, a sugar molecule, is commonly found on the surfaces of numerous pathogens. The presence of mannose receptors makes mannose pivotal for diverse processes, such as receptor-mediated endocytosis and phagocytosis.[16–18] Therefore, mannosylated nanoparticles may target APCs expressing

[a] Department of Virology, College of Veterinary Medicine and Research Institute for Veterinary Science, Seoul National University, Seoul 08826, Republic of Korea. E-mail: sds@snu.ac.kr

[b] Department of Chemical and Biomolecular Engineering, Yonsei University, Yonsei-ro 50, Seoul, 03722, Republic of Korea. E-mail: haam@yonsei.ac.kr

† Electronic supplementary information (ESI) available. See DOI: https://doi.org/10.1039/d5ma00115c

‡ These authors contributed equally.

mannose receptors and selectively deliver Ags through mannose-mediated mechanisms. Previous studies have also suggested that the mannosylation of drugs enhances MHC class I and II Ag presentation as well as T-cell stimulation compared to those of their non-mannosylated counterparts, thereby boosting Ag-specific immune responses.[16,19]

Incorporating various immunostimulants into vaccines as adjuvants is crucial for enhancing immunogenicity. Furthermore, nanoparticulate systems offer a promising avenue for delivering immunostimulants more efficiently to their targets and shielding them from biodegradation in the physiological environment, thereby eliciting potent immune responses. Resiquimod, also known as R848, is a member of the imidazoquinolinone family and functions as an agonist of toll-like receptors 7 and 8 (TLR7/8). This small molecule primarily engages TLR7/8, the main pattern-recognition receptors expressed on the endosomes of APCs.[20] Activation by specific ligands can prompt the production of inflammatory cytokines such as interleukin-6 (IL-6) and tumor necrosis factor-alpha (TNF-α), thus eliciting the immunogenicity of vaccines. However, the poor water solubility of R848 makes its effective delivery and uptake by APCs challenging. Nanoparticle-based delivery systems improve the bioavailability and cellular uptake of hydrophobic compounds such as R848. Furthermore, the intracellular localization of TLR7/8 within endosomes presents an opportunity to enhance immune response activation through nanoparticle-mediated delivery.[21,22] Delivery of R848 within nanoparticles facilitates intracellular trafficking to endosomes, thereby promoting efficient engagement with TLR7/8 and subsequent immune stimulation.

In this context, we engineered a mannosylated nanoparticulate vaccine delivery system using DSPE-PEG-mannose to enhance the delivery efficacy and immunogenicity of vaccines by selectively targeting APCs. We developed mannose-decorated polymer bilayer nanoparticles (Man-PSomes), which encapsulate both Ags and immunostimulants.[9] Amphiphilic polymers self-assemble to form bilayer spherical polymersomes (PSomes), which are advantageous in vaccine delivery platforms for the co-delivery of molecules.[23–25] Hydrophilic Ag is encapsulated in the inner core of PSomes, whereas water-insoluble R848 can be within the bilayer of the hydrophobic membrane. Man-PSomes co-encapsulated with ovalbumin (OVA) and R848 (OVA/R848/Man-PSomes) induced potent immune responses *in vitro* and *in vivo* (Fig. 1). Man-PSomes enhanced payload uptake *via* mannose-mediated endocytosis, leading to enhanced Ag and R848 delivery efficacy and presentation of Ag through the cytosolic processing pathway, thereby inducing the increased expression of pro-inflammatory cytokines and co-stimulatory molecules. We further demonstrated that intramuscular immunization with OVA/R848/Man-PSomes induced enhanced Ag-specific humoral and cellular responses in mice compared to those of formulations containing soluble Ag and PSomes without mannose. Man-PSomes, which are composed of biocompatible polymers, not only offer a safe and stable vaccine formulation strategy by simultaneously co-encapsulating protein Ags and immunostimulants, but also provide a powerful and versatile platform that
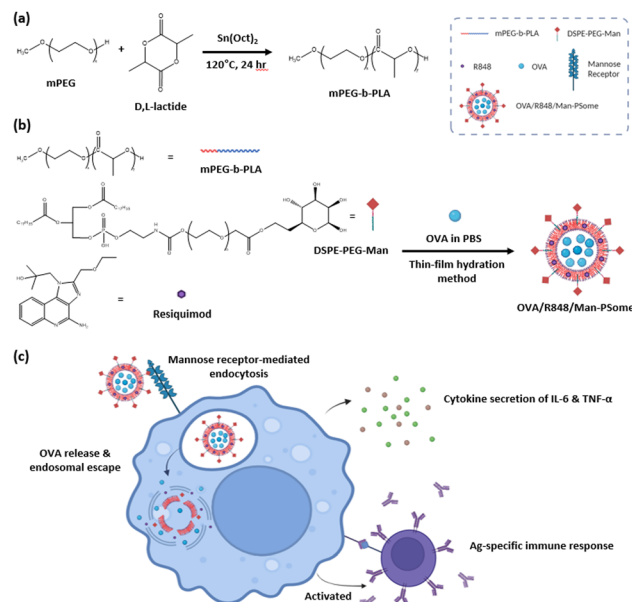

Fig. 1 Schematic diagram of the synthesis of (a) mPEG-*b*-PLA co-polymers through ring-opening polymerization. (b) Design of a Man-PSome containing both OVA and R848 (OVA/R848/Man-PSome). (c) Illustration of enhanced cellular Ag uptake by APCs induced by OVA/R848/Man-PSomes, secretion of IL-6 and TNF-α by activated APCs, and Ag-specific antibody immune response-based humoral and cellular immunity.

induces strong humoral and cellular immune responses, thus meeting public health demands for vaccine development against infectious diseases.

Experimental

Materials

Methoxy-poly(ethylene glycol) (mPEG) with a molecular weight of 2000 Da, D,L-lactide (3,6-dimethyl-1,4-dioxane-2,5-dione), and stannous octoate (Sn(Oct)₂) were obtained from Sigma-Aldrich (St. Louis, MO, USA). R848 was purchased from InvivoGen (San Diego, CA, USA), and DSPE-PEG-mannose was obtained from Biopharma PEG (Watertown, MA, USA). Dulbecco's phosphate-buffered saline (DPBS; 10 mM, pH 7.4), Dulbecco's modified Eagle's medium (DMEM), ovalbumin, ovalbumin–fluorescein conjugate, and ovalbumin–Alexa Fluor™ 488 conjugate were purchased from Thermo Fisher Scientific (Waltham, MA, USA). Diethyl ether was purchased from Duksan Pure Chemicals Co. Ltd. (Ansan, South Korea). Horseradish peroxidase (HRP)-conjugated goat anti-mouse IgG, IgG1, and IgG2a antibodies were purchased from Abcam (Cambridge, UK). Enzyme-linked immunosorbent assay (ELISA) kits for investigating IL-6 and TNF-α levels were purchased from R&D Systems (Minneapolis, MN, USA). Antibodies and markers for flow cytometry analysis were purchased from BioLegend (San Diego, CA, USA). All the other chemicals and reagents were of analytical grade.

Synthesis of mPEG-*b*-PLA

The amphiphilic copolymer mPEG-*b*-PLA was synthesized by the ring-opening polymerization of D,L-lactide with mPEG as

the initiator. Varying mass fractions of mPEG were obtained by changing the molar ratio of D,L-lactide to mPEG. To begin the synthesis, mPEG and D,L-lactide were introduced into a 3-neck flask with anhydrous toluene as the solvent. Polymerization was conducted at 120 °C for 18 h with continuous nitrogen purging and vigorous stirring, and Sn(Oct)$_2$ was used as a catalyst.[26] After the reaction, the solvent was removed by rotary evaporation, and the product solution was precipitated repeatedly in cold diethyl ether using a Buchner funnel. After purification, mPEG-*b*-PLA was vacuum-dried at room temperature for 2 days. To verify its successful synthesis, the polymer was characterized by Fourier-transform infrared (FT-IR) spectroscopy (Excalibur Series, Varian Inc., USA), ^{1}H-nuclear magnetic resonance (NMR) spectroscopy (400 MHz NMR Spectrometer, Bruker, Germany), and gel permeation chromatography (GPC) (YOUNG-LIN ACME HPLC System, Young Lin Instrument Co., Korea). The molecular weights of the synthetic mPEG-*b*-PLA and f_{mPEG} values were determined using ^{1}H-NMR and GPC. f_{mPEG} is the calculated mass fraction of mPEG in mPEG-*b*-PLA, estimated as follows:

$$f_{mPEG} = \frac{Mass_{mPEG}}{Mass_{PLA} + Mass_{mPEG}}$$

Preparation and characterization of polymersomes

A thin-film hydration method described in previous studies was used to prepare OVA/R848/Man-PSomes.[9,24,27] More specifically, to prepare 3 mL of dispersion, 5 mg of mPEG-*b*-PLA, 90 μg of DSPE-PEG-mannose, and 60 μg of R848 were dissolved in 1 mL of chloroform. The organic solvent was removed *via* rotary evaporation. Following 5 h of solvent evaporation, the polymer thin film was hydrated overnight with 3 mL of DPBS under 60 °C. After cooling, 120 μg of OVA was added to the DPBS solution, and vigorously stirred at 25 °C for 5 h. Since the range of nanoparticle size distribution is rather large, filter extrusion was conducted using a hydrophilic PTFE syringe filter with 0.45 μm pore size. To remove excess OVA or R848 that was not encapsulated in the nanoparticles and collect the purified products, we used Amicon centrifugal filtration. OVA/R848/Man-PSomes were concentrated and collected *via* ultracentrifugal filtration, using 100 kDa MWCO Amicon filters. The hydrodynamic size and zeta potential of the prepared PSomes and Man-PSomes were measured using dynamic light scattering (DLS; ELSZ-2000ZS, Otsuka Electronics, Osaka, Japan) and nanoparticle tracking analysis (NTA; NanoSight NTA, Malvern Panalytical, Malvern, UK), and the morphology of the PSome and Man-PSome were evaluated *via* transmission electron microscopy (TEM; JEM-1011, JEOL, Tokyo, Japan).

Quantification of OVA loading

The concentration of encapsulated ovalbumin was determined using fluorescence intensity measurements and a bicinchoninic acid (BCA) protein assay. Fluorescein isothiocyanate (FITC)-labeled OVA (OVA-FITC) was used to synthesize OVA-FITC/R848/Man-PSome. OVA-FITC (1 mg mL^{-1}) was diluted 2-fold for use as the standard with concentrations ranging from 100 to 7.8125 μg mL^{-1}. The levels of OVA-FITC incorporated in the

PSomes were detected by measuring the fluorescence spectra at 485 nm excitation and 520 nm emission wavelengths. Encapsulation efficiency (EE) was calculated as follows:

$$EE\,(\%) = \frac{Mass\;of\;OVA\;in\;final\;product}{Mass\;of\;total\;feedings\;of\;OVA} \times 100$$

To cross-check the loading content of OVA, a BCA assay was performed using OVA/R848/Man-PSomes and OVA (1 mg mL^{-1}). OVA/R848/Man-PSomes were fabricated as per the method mentioned previously, and BCA assay was conducted according to the manufacturer's instructions (Pierce™ BCA protein assay kit, Thermo Scientific™, Waltham, MA, USA). Briefly, protein concentration was determined at an absorbance of 562 nm using a microplate reader (Molecular Devices, Sunnyvale, CA, USA).

Quantification of R848 loading

The concentration of R848 was quantified by liquid chromatography–tandem mass spectrometry (LC-MS; Q Exactive Plus LC-MS, Thermo Fisher Scientific). Specifically, the LC mode was tested with an Ultimate 3000 RS UHPLC (Thermo Fisher Scientific) and the MS mode with Q-Exactive Orbitrap Plus (Thermo Fisher Scientific). Samples containing R848 were dissolved in chloroform, and a gradient mode was applied with solvent A (distilled water containing 0.1% formic acid) and solvent B (acetonitrile containing 0.1% formic acid). Specifically, the samples were chromatographically separated using the gradient mode as follows: 90% solvent A and 10% solvent B for 1.5 min, then 0% solvent A for 10 min, maintenance of 0% A and 100% B for 4 min, then a return to the initial condition for 14.5 min, and retention for 17 min. The flow rate was maintained at 400 μL min^{-1} with an injection volume of 5 μL, and the column temperature was set to 45 °C. The temperature of the sampler was adjusted to 5 °C during the whole operation. The column was Acquity UPLC BEH C18, (1.7 μm, 2.1 × 100 mm). The R848 peak was well-separated under the established chromatographic conditions.[28]

The mass spectrometer was operated in the positive ion mode with a sheath gas flow rate of 50 L min^{-1} and an auxiliary gas flow rate of 13 L min^{-1}. The optimization of the tuning parameters was conducted by direct infusion of R848 standard solution as follows: spray voltage of 3500 V and capillary temperature of 370 °C.

R848 was detected at a wavelength of 320 nm, and its concentration was calculated by calibration using standard solutions. The EE of R848 was determined using the following equation:

$$EE\,(\%) = \frac{Concentration\;of\;R848\;in\;final\;product}{Concentration\;of\;total\;feedings\;of\;R848} \times 100$$

Release profiles of OVA

The release profile of OVA was further evaluated *via* dialysis in a physiological environment. Alexa Fluor 488 conjugated with OVA (OVA-AF488) was used to prepare OVA-AF488/R848/Man-PSome. OVA-AF488/R848/Man-PSome was synthesized as

described previously. OVA-AF488 and OVA-AF488/R848/Man-PSome solutions were sealed in a dialysis membrane with an MWCO of 100 kDa. Dialysis tubes were immersed in 5 mL of PBS (pH 7.4) and incubated at 37 °C under continuous moderate shaking at 150 rpm in the dark. At fixed time intervals, the entire solution was collected, and an equal volume of fresh PBS was added to maintain a constant volume. Release profiles were monitored for 72 h. The cumulative release of OVA-AF488 was detected using fluorescence spectra at 485 nm excitation and 520 nm emission wavelengths. The OVA-AF488-only group was used for control experiments.

Cell viability of mPEG-*b*-PLA and DSPE-PEG-mannose

Murine macrophages (RAW264.7 cells) were seeded (4×10^4 cells per well) onto a 96-well cell culture plate (SPL Life Sciences Co., Ltd., Pocheon, South Korea) and then incubated at 37 °C in an atmosphere of 5% CO_2. To verify the potential cytotoxicity of the polymers used in this study, the cells were incubated with mPEG-*b*-PLA and DSPE-PEG-mannose at different concentrations for 18 h. *In vitro* cell viability assay was performed using a cell counting kit (EZ-Cytox Cell Viability Assay Kit; DoGenBio, Seoul, South Korea) according to the manufacturer's instructions.

Static hemolysis of chicken red blood cells

Chicken red blood cells (RBCs) were diluted to 1% with PBS, and this 1% RBC solution was transferred to a U-bottom 96-well plate (50 μL per well) and 50 μL of serially diluted samples were treated and incubated with RBCs for 1 h at 37 °C. OVA/R848/Man-PSomes were serially diluted 2-fold to obtain solutions with a concentration range of 2^{-9}–2^{0} μg mL^{-1}. In this analysis, PBS was used as a negative control, and 1% v/v Triton-X 100 in PBS was used as a positive control. Following incubation, the absorbance spectra measurement at 350–500 nm was obtained using a SpectraMAX i3x Multi-Mode Detection Platform microplate reader (molecular devices) at a maximum absorbance intensity peak of 410 nm. The percentage of hemolysis was calculated using the following equation:

$$\text{Hemolysis}\,(\%) = \frac{\text{Abs}_{\text{test}} - \text{Abs}_{\text{NC}}}{\text{Abs}_{\text{PC}} - \text{Abs}_{\text{NC}}} \times 100$$

Ag uptake efficacy of PSomes in APCs

Bone marrow dendritic cells (BMDCs) were extracted from the femurs of six-week-old BALB/c female mice using a previously established method.[29]

For flow cytometric analysis, RAW264.7 cells or BMDCs were seeded in 6-well plates (1×10^6 cells per well) and incubated for 24 h at 37 °C in an atmosphere of 5% CO_2. To verify the specificity of the mannose moiety binding to APCs, a mannose inhibition test was performed to block their mannose receptors. RAW264.7 cells or BMDCs were treated with or without 2 mg mL^{-1} of D-(+)-mannose solution for 1 h and then incubated with PSomes and Man-PSomes treated with 2 μg OVA-FITC or -AF488 per well at 37 °C for 4 h. Subsequently, the harvested cells were washed with PBS and subjected to flow cytometry using

an LSR II flow cytometer (BD Biosciences, Santa Clara, CA, USA) and analysis using FlowJo software.

The intracellular localization of Ag in RAW264.7 cells or BMDCs was observed using confocal laser scanning microscopy (CLSM). RAW264.7 cells or BMDCs were seeded in a confocal dish (4×10^5 cells per dish) and incubated at 37 °C in an atmosphere of 5% CO_2 for 18 h. Subsequently, OVA-AF488 solution and OVA-AF488-encapsulating PSomes and Man-PSomes were added to the dishes and cultured for 4 h. After washing twice with cold PBS, cells were cultured in a medium containing LysoTracker-Red DND-99 (Molecular Probes, Eugene, OR, USA) and Hoechst (Molecular Probes) in the dark to label the lysosomes and nuclei, respectively. After incubation, the cells were washed with PBS and fixed with 2% formaldehyde solution at 4 °C for 20 min. Finally, cellular uptake of the particles was visualized using a Zeiss LSM 980 confocal laser scanning microscope (Carl Zeiss, Jena, Germany).

In vitro analysis of cytokine secretion levels by ELISA

RAW264.7 and BMDCs were prepared according to conventional protocols and cultured in 96-well cell culture plates (2×10^4 cells per well). The cells were stimulated with PBS or different concentrations of OVA, R848, PSomes, Man-PSomes, OVA/R848/Psomes, or OVA/R848/Man-PSomes for 18 h. Supernatants were collected, and the expression of IL-6 or TNF-α were examined using ELISA kits (R&D Systems) according to the manufacturer's instructions.

Cross presentation analysis of co-stimulatory molecules *in vitro*

To evaluate BMDC activation, the cells were incubated overnight with PBS, OVA/R848, OVA/R848/PSomes, or OVA/R848/Man-PSomes. Then, cells were collected and blocked with anti-mouse CD16/CD32 (Cat: 156604, clone S17011E, BioLegend) for 20 min at 4 °C. After blocking, the cells were stained with anti-CD11c-FITC (BioLegend), anti-CD40-PE (BioLegend), and anti-CD80-APC (BioLegend) antibodies at 4 °C for 1 h. Unbound antibodies were removed by centrifugation, and the cells were fixed with 2% formaldehyde solution at 4 °C for 20 min. After a final wash and resuspension, the cells were analyzed using flow cytometry (SH800S cell sorter, Sony).

Animal immunization studies

Female BALB/c mice aged 7 weeks were obtained from Daehan Biolink Co. Ltd. (Seoul, South Korea) and housed under pathogen-free conditions with a 12/12 h light/dark cycle, temperature of 23 ± 2 °C, and relative humidity of 50 ± 10%.

The mice were randomly divided into 5 groups ($n = 5$ per group) and vaccinated with 50 μL per dose of PBS (control), OVA (10 μg), OVA/R848/PSomes (10 μg of OVA and 16.7 μg mL^{-1} of R848), or OVA/R848/Man-PSomes (10 μg of OVA and 16.7 μg mL^{-1} of R848) *via* intramuscular injection in the rear quadriceps on day 0 and 14. Blood was collected from the mice *via* the retro-orbital plexus two weeks after each injection (days 14 and 28). Serum was obtained from the blood by centrifuging it for 10 min at 2500 rpm. To assess T-cell immune responses, the spleens were harvested from immunized mouse on day 28

immediately after euthanizing them *via* CO_2 asphyxiation. All experimental procedures were approved by the Chonnam National University Institutional Animal Care and Use Committee (approval number: CNU IACUC-YB-2023-115; date of approval: August 30, 2023) and conducted in accordance with institutional guidelines.

Ag-specific antibody analysis by ELISA

To assess the induction levels of Ag-specific antibodies, the titers of OVA-specific IgG and its subtypes (IgG1 and IgG2a) were analyzed by ELISA using serum samples collected from each mouse ($n = 5$). Briefly, 96-well immuno-plates were coated with 100 ng of OVA (100 μL per well) overnight at 4 °C and then blocked for 1.5 h at room temperature by adding blocking buffer (5% skimmed milk in distilled water). Plates were rinsed three times with washing buffer (0.01% v/v Tween20 in PBS) and then incubated with serially diluted sera for 2 h at room temperature. Thereafter, 100 μL of HRP-labeled goat anti-mouse IgG, IgG1, or IgG2a antibodies (1:50 000 diluted in 3% skim milk) were added into wells and incubated for another 2 h at room temperature. Next, 100 μL of TMB substrate solution was added to each well and incubated for 30 min at room temperature. The enzyme reactions were terminated using 1 M H_2SO_4 (50 μL per well), and the absorbance was recorded by using a SpectraMAX i3x Multi-Mode Detection Platform microplate reader (molecular devices) at a wavelength of 450 nm. The endpoint titer was determined using an optical density (O.D.) cut-off value of 0.05, which was the O.D. of the blank.

Isolation of splenocytes and assessment of T-cell response *ex vivo*

Two weeks after the final vaccination, immunized mice from each group were sacrificed, and their spleens were harvested. The spleens were homogenized in RPMI 1640 culture medium supplemented with 2 mM L-glutamine, 10% FBS, 3% penicillin/streptomycin, 1% non-essential amino acids, 10 mM HEPES, 1 mM sodium pyruvate, and 50 μM beta-mercaptoethanol. The homogenization process involved mashing and pressing the plunger end of a syringe on ice, followed by processing into single-cell suspensions using a strainer. The splenocytes were washed and resuspended in RBC lysis buffer. After washing with cold PBS, the splenocytes were resuspended in the culture medium. Splenocytes (5×10^5 cells per well) were incubated for 96 h at 37 °C with 100 ng of OVA as a stimulant. Supernatants were collected, and IFN-γ concentration was analyzed by using ELISA kits (R&D Systems) according to the manufacturer's instructions.

To evaluate intracellular cytokine staining, splenocytes were isolated from vaccinated mice and restimulated with Ag for 4 h. IFN-γ-producing $CD4^+$ and $CD8^+$ T cells were quantified by flow cytometry. GolgiPlug (BD Biosciences) was added to inhibit intracellular transport of cytokines and the splenocytes were then incubated for an additional 4 h. Cells were blocked with anti-CD16/CD32 antibody (Biolegend, San Diego, CA, USA) for 20 min at 4 °C and then immunostained with anti-CD4 PE and anti-CD8a APC antibodies for 20 min at 4 °C. For intracellular cytokine staining, cells were permeabilized using a Cytofix/Cytoperm solution (BD Biosciences) and incubated with the anti-IFN-γ APC/Cy7 antibody. Samples were then washed and analyzed by flow cytometry.

Results and discussion

Preparation and characterization of Polymers

To use PSomes as a construct, a copolymer of mPEG-*b*-PLA was synthesized as previously described.[9,23] The co-polymer mPEG-*b*-PLA is well known for its biocompatibility and biodegradability, which makes it suitable for extensive use in biomedical and pharmaceutical applications.[30–32] Briefly, mPEG-*b*-PLA was synthesized by ring-opening polymerization of D,L-lactide monomers with hydroxyl groups at the ends of mPEG. The hydrophobic-to-hydrophilic components of the block copolymer, *i.e.*, the f_{mPEG} value of mPEG-*b*-PLA, can be adjusted by changing the molar ratio of D,L-lactide to mPEG. In this study, we synthesized two block co-polymers, mPEG-*b*-PLA #1 and mPEG-*b*-PLA #2, with f_{mPEG} values of 0.256 and 0.429, respectively (Table S1, ESI†). Successful polymerization was confirmed by ^{1}H-NMR and FT-IR spectroscopy. Fig. S1a (ESI†) shows the FT-IR spectra of mPEG, D,L-lactide, and mPEG-*b*-PLA. The characteristic absorption band at 2902 cm^{-1} corresponds to the stretching vibration of methoxy (–O–CH$_3$–) in mPEG. Carboxy (–C=O–) and hydroxy (–OH–) stretches of lactide appear at 1760 and 1470 cm^{-1} of mPEG-*b*-PLA, respectively. As shown in Fig. S1b (ESI†), prominent peaks at 5.17 ppm (CH in PLA) and 3.38 ppm (CH$_3$O in mPEG) confirm the successful polymerization of mPEG-*b*-PLA. As shown in Fig. S1c (ESI†), the mPEG-*b*-PLA samples exhibited clear, sharp, and single peaks with a leftward shift, indicating the successful polymerization of mPEG-*b*-PLA.

Preparation and characterization of PSomes

First, Man-PSomes were fabricated using the thin-film hydration method, resulting in Man-PSomes #1 and Man-PSomes #2 bilayer nanoparticles, which were synthesized from mPEG-*b*-PLA #1 and mPEG-*b*-PLA #2, respectively. As shown in Fig. S2 (ESI†), different nanostructures were fabricated based on the range of f_{mPEG} values. Consistent with previous studies, we found that bilayer spherical nanoparticles form when the f_{mPEG} value is ≤0.3.[33] Man-PSomes #1 were spherical bilayer polymersomes with uniform homogeneity. However, Man-PSomes #2 exhibited a variety of structures, including micelles and tubular and spherical polymersomes. Man-PSome #1 was selected for subsequent *in vitro* and *in vivo* experiments because it exhibited narrow homogeneity with a low polydispersity index (PDI) of 0.127 (Table S2, ESI†).

Three major components constitute the Man-PSome formulation, as shown in Fig. 1. First, hydrophilic OVA was encapsulated in the aqueous inner core of Man-PSomes. Next, hydrophobic R848 was incorporated between the bilayers of amphiphilic polymers, constructing a membrane with a spherical
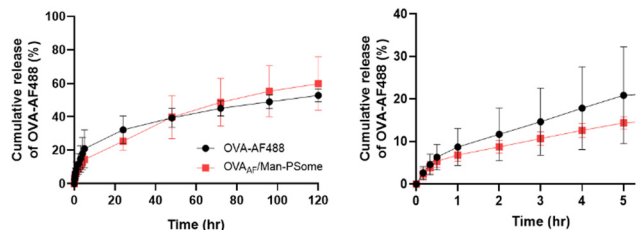
Fig. 3 Release profiles of OVA-AF488 from OVA$_{AF}$/Man-PSome and OVA-AF488 only in PBS (pH 7.4) at 37 °C. Data are presented as mean ± S.D. (*n* = 3). The amount of released OVA-AF488 was monitored for 120 h by measuring the fluorescence intensity at 485 nm excitation and 520 nm emission wavelengths.

release rate than the soluble Ag-only group. Therefore, the sustained release of OVA from Man-PSomes could indicate the potency of the enhanced Ag-specific immune response by allowing a more prolonged and controlled presentation of antigens to the immune system.[41]

In vitro cytotoxicity test of polymers and hemolysis analysis of polymersomes

To validate the cytotoxicity of the Man-PSomes, each polymer was evaluated using an *in vitro* cell viability assay. After incubating the RAW264.7 cells for 18 h, no significant cytotoxicity was observed in any of the experimental groups at any concentration tested (Fig. S6, ESI†). Therefore, the biosafety of the polymer was verified, demonstrating the biocompatibility and potential cytocompatibility of the nanoparticles as carriers for vaccine delivery platforms.

Furthermore, a hemolysis assay was conducted to assess the potential toxicity or adverse hemolytic effects of Man-PSomes on RBCs and, by extension, on the circulatory system. Because RBCs are affected by everything that is absorbed into the bloodstream, the hemoglobin released upon RBC lysis can be a measure of the impact of OVA/R848/Man-PSomes on erythrocytes. Hemocompatibility test was performed by exposing 1% chicken RBC solution to varying concentrations of OVA/R848/Man-PSomes. As shown in Fig. S7 (ESI†), OVA/R848/Man-PSomes hardly caused hemolysis, indicating that they did not possess any hemolytic toxicity. These results suggest that Man-PSomes and their components exhibit minimal cytotoxicity and do not disrupt the normal biochemical environment of cells.

OVA uptake efficacy of Man-PSomes *in vitro* & *in vivo*

The cellular uptake of Ags by APCs is crucial for bridging innate and adaptive immunity. When vaccinated, the organism first engages the innate immune system, followed by the adaptive immune system. Increasing the adaptive immune response of an organism to trigger a stronger immune response against pathogens is an effective approach. For a vaccine to efficiently elicit adaptive immunity and confer immune protection *in vivo*, it must be readily taken up and processed by APCs. Thus, the efficacy of cellular Ag uptake by Man-PSomes, which target APCs *via* the mannose receptor, was quantitatively evaluated using RAW264.7 macrophages and BMDCs *via* flow cytometry.

OVA labeled with FITC or AF488 tracker was used as a model Ag. As shown in Fig. 4a, b and Fig. S8a, b (ESI†), the results indicate that Man-PSomes had a significant increase in Ag cellular uptake, with mean fluorescence intensity (MFI) values 4.1 and 4.45 times higher than those of soluble OVA alone in RAW264.7 and BMDCs, respectively. Furthermore, Man-PSomes delivered a higher quantity of Ag to APCs than PSomes without the mannose moiety.

A mannose receptor inhibition test was conducted to verify the mannose receptor-mediated targeting of OVA/R848/Man-PSomes. D-(+)-mannose was administered prior to exposure to OVA/R848/Man-PSomes or OVA/R848/PSomes to block the receptors on the APCs. As shown in Fig. 4c and Fig. S8c (ESI†), there was no significant difference in cellular Ag uptake by PSomes without a mannose moiety, whereas Man-PSomes showed a prominent decrease in cellular uptake. Furthermore, CLSM images revealed a weak green OVA signal in RAW264.7 cells pretreated with mannose, indicating reduced Ag uptake due to receptor blocking (Fig. S9, ESI†). In contrast, cells not

Fig. 4 Cellular uptake of nanoparticles by RAW264.7 cells measured by OVA-FITC- or OVA-AF488-positive cells using flow cytometry and CLSM. (a) MFI of RAW264.7 after incubation with negative control (cell media), OVA-FITC, OVA-FITC/PSome, or OVA-FITC/Man-PSome. One-way ANOVA Dunnett's test was used for statistical analysis. Data are presented as mean ± S.D. (*n* = 3; ****p < 0.0001). (b) Gray, red, green, and blue histograms represent the cells treated with negative control, OVA-FITC, OVA-FITC/PSome, and OVA-FITC/Man-PSome, respectively. (c) *In vitro* evaluation of cellular Ag uptake efficacy for PSome and Man-PSome following mannose pretreatment of RAW264.7 to block mannose receptors. (d) CLSM images of RAW264.7 cells treated with negative control, OVA-AF488, OVA-AF488/PSome, and OVA-AF488/Man-PSome for 4 h at 37 °C. Scale bars indicate 50 μm.

pretreated with mannose exhibited a strong green OVA signal, consistent with the flow cytometry results. These results demonstrate that mannose-decorated nanoparticles can efficiently promote cellular Ag uptake by APCs through the mannose receptor-targeting moieties.

As a qualitative analysis, Ag endocytosis efficiency was visualized through CLSM images of RAW264.7 macrophages and BMDCs (Fig. 4d and Fig. S8d, ESI†). The strongest fluorescence signal from OVA-AF488 was observed in both RAW264.7 macrophages and BMDCs treated with OVA/R848/Man-PSomes, compared to that of other groups. These results were consistent with the quantitative results of cellular Ag uptake, suggesting that Man-PSomes were effectively internalized by APCs. Overall, these results demonstrate that Man-PSomes are an effective nanoparticulate vaccine delivery system and confirm the specificity of mannose receptor-mediated targeting of APCs.

Further, we evaluate Ag retention *in vivo* by intramuscularly injecting mice with AF647-labeled OVA either in its soluble form or with OVA-AF647/R848/Man-PSomes. At 5 h post-injection, we performed *in vivo* fluorescence imaging to assess Ag retention. The Man-PSome group displayed a bright, well-defined depot at the injection site, whereas free OVA-AF647 was diffusely dispersed (Fig. S10(a), ESI†). Quantitative analysis of the accumulated fluorescence intensity within the defined ROI confirmed significantly higher signal retention for the Man-PSome formulation compared with that of the soluble antigen (Fig. S10(b), ESI†). These results demonstrate that mannose functionalization and nanoparticulate delivery substantially prolong antigen residence, thereby enhancing uptake by APCs.

Secretion of immunostimulatory cytokines by APC activation

To assess the activation of APCs *in vitro*, secretion of pro-inflammatory cytokines IL-6 and TNF-α were analyzed in RAW264.7 macrophages and BMDCs. R848 is a TLR7/8 agonist. TLR 7 and 8 are endosomal transmembrane receptors that induce cytokine production upon activation. We explored whether a vaccine delivery system that enhances the delivery of R848 to TLR 7 and 8 on APCs increases cytokine expression levels.[20] To verify the immunostimulatory effect of R848, RAW 264.7 cells and BMDCs were treated with PBS, OVA, R848, Man-PSomes, OVA/R848/Psomes, or OVA/R848/Man-Psomes. After 18 h of incubation, supernatant was collected and IL-6 and TNF-α secretion levels were analyzed by ELISA. As shown in Fig. 5a, the secretion of both cytokines was significantly higher in the OVA/R848/Man-PSome treatment group compared to the that of other groups. The expression levels of IL-6 and TNF-α induced by OVA/R848/Man-PSomes in BMDCs were 2.68- and 3.43-fold higher than those induced by mannose non-targeted OVA/R848/PSome group, respectively, suggesting that mannose-mediated delivery enhancement can more effectively activate APCs. In addition, negligible levels of cytokine expression were observed in the OVA and Man-PSome groups, indicating that the inflammatory response was driven by immunostimulants and not induced by nanoparticles or Ag. We estimated the cytokine expression levels in RAW264.7 macrophages and found very similar results to those observed in RAW264.7 macrophages
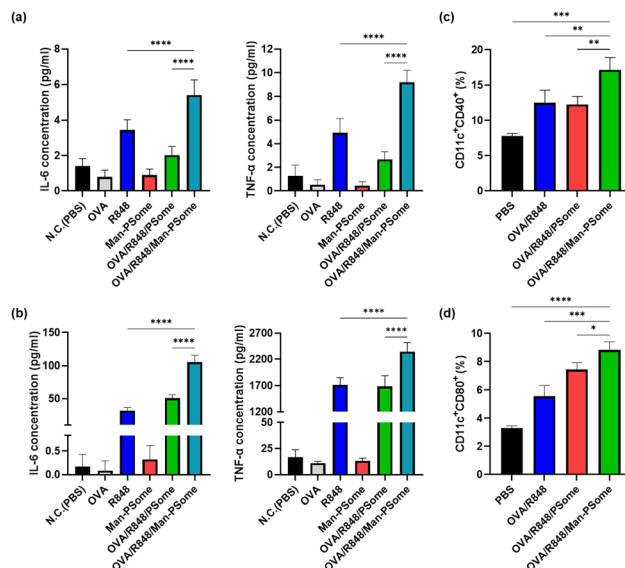

Fig. 5 Quantitative comparison of IL-6 and TNF-α induction in (a) BMDCs and (b) RAW264.7. Expression levels of IL-6 and TNF-α in BMDCs and RAW264.7 stimulated with negative control (PBS), OVA-only, R848-only, Man-PSomes, OVA/R848/PSomes, and OVA/R848/Man-PSomes, as determined by ELISA. The frequencies of the (c) clusters of differentiation 40+ (CD40+) and (d) 80+ (CD80+) of the BMDCs treated with PBS, OVA/R848, OVA/R848/PSomes, and OVA/R848/Man-PSomes are presented. One-way ANOVA Dunnett's test was used for statistical analysis. Data are presented as mean ± S.D. ($n = 5$; *p, 0.05, **$p < 0.01$, ***$p < 0.001$, and ****$p < 0.0001$).

(Fig. 5b). Quantitative investigation of cytokine induction reveals that OVA/R848/Man-PSome effectively facilitates the delivery of R848 to APCs *via* mannose receptor-targeted endocytosis, enabling its access to TLR 7 and 8 within the APC endosomes, thus increasing the immunostimulatory activity of APCs.

Furthermore, to analyze the maturation of APCs for increased T cell activation, we assessed the expression levels of co-stimulatory surface molecules, such as clusters of differentiation 40 (CD40), 80 (CD80), and 86 (CD86), in BMDCs using flow cytometry. The engagement of these surface molecules stimulates T cells to cross-present Ags, initiating CD8+ T cell immunity and promoting the development of durable memory T cells.[42] BMDCs treated with OVA/R848/Man-PSomes displayed significantly larger populations expressing costimulatory surface proteins (CD40, CD80, and CD86) than those treated with OVA/R848 and OVA/R848/Man-PSome (Fig. 5c, d and Fig. S11, ESI†). These results suggest that OVA/R848/Man-PSomes elicit potent immune responses through the maturation and activation of APCs, demonstrating their considerable potential as both antigen and immunostimulant delivery agents. Moreover, the superior *in vitro* immunogenicity of Man-PSomes compared to non-mannosylated PSomes indicates that targeting APCs through mannose-mediated cell uptake offers significant advantages for vaccine delivery systems.

OVA-specific immune response elicited by Man-PSomes *in vivo*

To evaluate the immune responses triggered by mannose-decorated nanoparticulate vaccine delivery systems *in vivo*,

BALB/c mice were vaccinated with PBS, OVA-only, OVA/R848/Psomes, or OVA/R848/Man-PSomes. Vaccination was administered twice intramuscularly, with a two-week interval between doses. Two weeks after each injection, sera from each group were collected (days 14 and 28) and antibody production levels were analyzed by ELISA. The levels of OVA-specific IgG antibodies in the serum after the booster dose (day 28) were higher across all groups than those after the first dose (day 14) (Fig. 6a). Notably, mice vaccinated with OVA/R848/Man-PSomes had significantly higher OVA-specific antibody titers than those in the other groups on days 14 and 28. Moreover, the group immunized with Man-PSomes showed significantly higher Ag-specific antibody production than the group immunized with non-mannosylated PSomes, confirming that differences in vaccine delivery efficacy, driven by the presence of moieties that target APCs, can affect the ability to generate humoral immune responses. To evaluate the production of IgG subclass antibodies in mouse sera, we assessed the levels of OVA-specific IgG1 or IgG2a induction two weeks after the final inoculation, which are indicative of Th2- and Th1-mediated immune responses, respectively. As shown in Fig. 6b, OVA/R848/Man-PSomes proved effective in producing both subclasses, along with an increase in total IgG, especially IgG2a. This indicates that the platform is highly effective in triggering Th1-type immunity, which is consistent with previous studies showing that R848 induces a substantial cellular immune response. The levels of OVA-specific IgG, IgG1, and IgG2a were higher in mice vaccinated with OVA/R848/Man-PSomes than in those receiving soluble OVA or non-mannosylated OVA/R848/PSomes. These outcomes may be attributed to the protective effect of the nanoparticulate structure on Ag and the sustained release of Ag, which enhances the immune response by prolonging the exposure of Ag to the

immune system. In addition, improved cellular delivery through the mannose receptor-targeted endocytosis of OVA/R848/Man-PSomes likely increased the immune activity of the system and enhanced the production of antibodies. Overall, these results suggest that Man-PSomes are capable of co-encapsulating Ags and a TLR7/8 agonist adjuvant and thus serve as potent nanoparticulate vaccine delivery systems to induce both humoral and cellular immune responses.

Ex vivo restimulation of isolated splenocytes

To confirm the superior immunostimulatory potential and Ag-specific cellular immune response elicited by OVA/R848/Man-PSomes, we conducted ex vivo Ag-restimulation of splenocytes. Two weeks after the final vaccination, immunized mice from each group were sacrificed and their splenocytes were isolated. Following restimulation with Ag for 96 h, the IFN-γ levels were significantly higher in mice vaccinated with OVA/R848/Man-PSomes compared to those vaccinated with soluble OVA or OVA/R848/PSome (Fig. 6c). This suggests that APC-targeted Man-PSome, which co-encapsulates Ag and the TLR7/8 agonist R848, effectively induces IFN-γ-secreting T cells and a Th1-mediated immune response in vaccinated mice, thereby markedly enhancing the adjuvant activity of R848.

Further, we performed intracellular cytokine staining to measure IFN-γ-producing $CD8^+$ and $CD4^+$ T cells using flow cytometry. While both OVA alone and OVA/R848/PSome showed low Ag-specific T cell responses, OVA/R848/Man-PSome led to an increase in the population of IFN-γ-secreting $CD8^+$ and $CD4^+$ T cells (Fig. S12, ESI†). Collectively, these results confirmed that Man-PSomes promote Th1 activation by inducing Ag-specific T cell responses, which may provide significant immune protection against pathogens.

Systemic and histopathological safety evaluation

Pro-inflammatory cytokines such as TNF-α and IL-6 are critical mediators of the acute inflammatory response, which manifests as fever and other symptoms associated with infection and inflammation. The cytokine release syndrome is a potential side effect of nanoparticle-based or adjuvant vaccines. To address this concern, we analyzed systemic cytokine levels in serum samples collected from immunized mice after vaccination. As shown in Fig. S13 (ESI†), the levels of TNF-α and IL-6 in the groups vaccinated with nanoparticles such as PSome and Man-PSome was similar to that observed in the PBS-treated control group. Notably, no significant increase in systemic cytokine levels was observed at either 1 or 4 days post-vaccination, indicating that the vaccine formulations do not induce overactivation of the inflammatory response.

Furthermore, we evaluated the histology of major organs, including the heart, liver, spleen, lungs, and kidneys, using hematoxylin and eosin staining to elucidate the safety profile of nanoparticulate delivery systems (Fig. S14, ESI†). According to our evaluation of the spleen, the occurrence of extramedullary hematopoiesis was minimal across all groups, including the negative control group, suggesting its unlikely association with the vaccine formulations. Furthermore, no significant
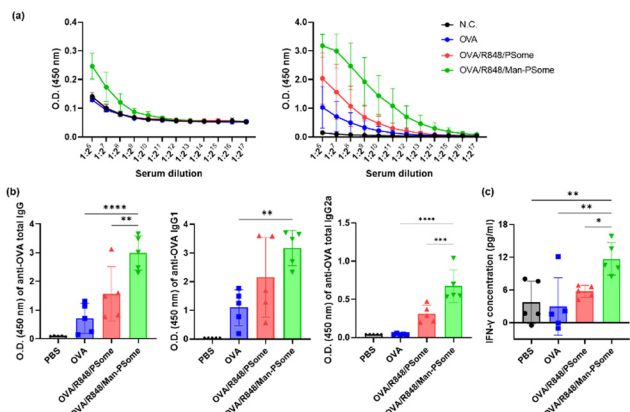

Fig. 6 (a) Quantitative comparison of OVA-specific total IgG induction in mice (n = 5 per group) 2 weeks after the first vaccination (left) and 2 weeks after the final vaccination (right). (b) Quantitative comparison of OVA-specific total IgG, IgG1, and IgG2a induction in mice (n = 5 per group) 2 weeks after the final vaccination. Induction of OVA-specific total IgG, IgG1, or IgG2a in mice vaccinated with PBS, OVA-only, OVA/R848/PSomes, and OVA/R848/Man-PSomes determined using ELISA at a serum dilution of 1 : 2.[7] (c) IFN-γ production by ex vivo restimulation of vaccinated mouse splenocytes with Ag. A One-way ANOVA Dunnett's test was used for statistical analysis. Data are presented as mean ± S.D. (n = 5; *p < 0.05, **p < 0.01, ***p < 0.001, ****p < 0.0001).

histopathological abnormalities were observed in other vital organs, confirming that the Man-PSome formulation did not induce detectable toxicity.

To further assess general systemic toxicity, we monitored body weight changes in immunized mice throughout the experimental period. As shown in Fig. S15 (ESI†), no significant weight loss was observed in OVA/R8484/Man-PSome vaccinated mice compared to that of the PBS-treated mice, indicating that the vaccine formulations did not induce general physiological stress or systemic adverse effects.

In addition, hematological and serum biochemical analyses were performed to evaluate potential hematotoxicity and organ dysfunction. Key hematological parameters—including white blood cell count, red blood cell count, hemoglobin concentration, and platelet count—remained within normal ranges and did not differ significantly among the groups (Table S6, ESI†). Likewise, serum biochemical markers such as aspartate aminotransferase (AST), alanine aminotransferase (ALT), blood urea nitrogen (BUN), and creatinine showed no abnormal increases, further confirming the absence of liver or kidney toxicity (Table S7, ESI†). These results collectively demonstrate the systemic safety and biocompatibility of the Man-PSome nanoparticle vaccine formulation.

Conclusions

In this study, we developed an effective vaccine delivery system that targets APCs via mannose receptors by fabricating a bilayer nanovesicle, termed Man-PSomes, using a biodegradable and biocompatible polymer. The surface of Man-PSomes was enriched with mannose to provide targeting moieties for APCs. This nanoparticle was capable of encapsulating both an antigen (OVA) and a TLR7/8 agonist adjuvant (R848). By targeting mannose receptors, which are abundant in macrophages and dendritic cells, this nanoparticulate vaccine increased Ag uptake by APCs in vitro. Additionally, OVA/R848/Man-PSomes demonstrated significantly higher efficiency in stimulating the maturation and activation of APCs, as evidenced by the increased expression of co-stimulatory molecules and the secretion of pro-inflammatory cytokines (IL-6 and TNF-α). In vivo immunization showed that OVA/R848/Man-PSomes significantly enhanced Ag-specific antibody responses. Improved T-cell-mediated immunity was observed after Ag restimulating splenocytes ex vivo, leading to increased production of the cytokine IFN-γ. Overall, these results indicate that the mannose-mediated vaccine delivery nanoparticle system can effectively enhance both humoral and cellular immune responses.

Nevertheless, this study has limitations. The use of OVA as a model antigen limits its clinical relevance. Therefore, future studies should use recombinant protein antigens to evaluate protective efficacy. Furthermore, data on the storage stability and scalability of nanoparticles for mass production remain insufficient, requiring further investigation to support the platform's translational potential.

Despite these limitations, our results lay a firm foundation for developing APC-targeted nanoparticulate platforms and highlight the potential of Man-PSomes as a promising delivery system for vaccines against infectious diseases and immunotherapy applications in tumor treatment.

Author contributions

J.-W. L. and S.-E. L. contributed equally to this work. Conceptualization: J.-W. L. and S.-E. L. Writing – original draft: J.-W. L. and S.-E. L. Data curation: J.-W. L. and S.-E. L. Validation: J.-W. L. and S.-E. L. Investigation: H. P and S. L. Formal analysis: M. Y. Supervision: D. S. and S. H.

Conflicts of interest

There are no conflicts to declare.

Data availability

The data supporting this article have been included as part of the ESI.†

Acknowledgements

Notes and references

1 B. Ju, Q. Zhang, J. Ge, R. Wang, J. Sun, X. Ge, J. Yu, S. Shan, B. Zhou, S. Song, X. Tang, J. Yu, J. Lan, J. Yuan, H. Wang, J. Zhao, S. Zhang, Y. Wang, X. Shi, L. Liu, J. Zhao, X. Wang, Z. Zhang and L. Zhang, Nature, 2020, 584, 115–119.

2 S. Okamura and H. Ebina, Vaccine, 2021, 39, 5719–5726.

3 T. Thanh Le, Z. Andreadakis, A. Kumar, R. Gómez Román, S. Tollefsen, M. Saville and S. Mayhew, Nat. Rev. Drug Discovery, 2020, 19, 305–306.

4 E. Kim, E. K. Lim, G. Park, C. Park, J. W. Lim, H. Lee, W. Na, M. Yeom, J. Kim, D. Song and S. Haam, Adv. Mater., 2021, 33, e2005927.

5 J.-W. Lim, Y.-R. Ahn, G. Park, H.-O. Kim and S. Haam, Pharmaceutics, 2021, 13, 1570.

6 P. Lung, J. Yang and Q. Li, Nanoscale, 2020, 12, 5746–5763.

7 J.-W. Lim, W. Na, H.-O. Kim, M. Yeom, G. Park, A. Kang, H. Chun, C. Park, S. Oh, V. P. Le, H. H. Jeong, D. Song and S. Haam, Adv. Healthcare Mater., 2019, 8, e1800953.

8 G. Park, W. Na, J.-W. Lim, C. Park, S. Lee, M. Yeom, E. Ga, J. Hwang, S. Moon, D. G. Jeong, H. H. Jeong, D. Song and S. Haam, ACS Nano, 2024, 18, 4847–4861.

9 J.-W. Lim, W. Na, H.-O. Kim, M. Yeom, A. Kang, G. Park, C. Park, J. Ki, S. Lee, B. Jung, H. H. Jeong, D. Park, D. Song and S. Haam, J. Mater. Chem. B, 2020, 8, 5620–5626.

10 M. S. Gebre, L. A. Brito, L. H. Tostanoski, D. K. Edwards, A. Carfi and D. H. Barouch, *Cell*, 2021, **184**, 1589–1603.

11 R. Tenchov, R. Bird, A. E. Curtze and Q. Zhou, *ACS Nano*, 2021, **15**, 16982–17015.

12 L. R. Baden, H. M. El Sahly, B. Essink, K. Kotloff, S. Frey, R. Novak, D. Diemert, S. A. Spector, N. Rouphael, C. B. Creech, J. McGettigan, S. Khetan, N. Segall, J. Solis, A. Brosz, C. Fierro, H. Schwartz, K. Neuzil, L. Corey, P. Gilbert, H. Janes, D. Follmann, M. Marovich, J. Mascola, L. Polakowski, J. Ledgerwood, B. S. Graham, H. Bennett, R. Pajon, C. Knightly, B. Leav, W. Deng, H. Zhou, S. Han, M. Ivarsson, J. Miller, T. Zaks and COVE Study Group, *N. Engl. J. Med.*, 2021, **384**, 403–416.

13 B. Nguyen and N. H. Tolia, *npj Vaccines*, 2021, **6**, 70.

14 Y. Ding, Z. Li, A. Jaklenec and Q. Hu, *Adv. Drug Delivery Rev.*, 2021, **179**, 113914.

15 M. Embgenbroich, H. J. P. van der Zande, L. Hussaarts, J. Schulte-Schrepping, L. R. Pelgrom, N. García-Tardón, L. Schlautmann, I. Stoetzel, K. Händler, J. M. Lambooij, A. Zawistowska-Deniziak, L. Hoving, K. de Ruiter, M. A. Wijngaarden, H. Pijl, K. Willems van Dijk, B. Everts, V. van Harmelen, M. Yazdanbakhsh, J. L. Schultze, B. Guigas and S. Burgdorf, *Proc. Natl Acad. Sci. U. S. A.*, 2021, **118**, e2103304118.

16 D. S. Wilson, S. Hirosue, M. M. Raczy, L. Bonilla-Ramirez, L. Jeanbart, R. Wang, M. Kwissa, J. F. Franetich, M. A. S. Broggi, G. Diaceri, X. Quaglia-Thermes, D. Mazier, M. A. Swartz and J. A. Hubbell, *Nat. Mater.*, 2019, **18**, 175–185.

17 F. Mastrotto, M. Pirazzini, S. Negro, A. Salama, L. Martinez-Pomares and G. Mantovani, *J. Am. Chem. Soc.*, 2022, **144**, 23134–23147.

18 J. M. Jaynes, R. Sable, M. Ronzetti, W. Bautista, Z. Knotts, A. Abisoye-Ogunniyan, D. Li, R. Calvo, M. Dashnyam, A. Singh, T. Guerin, J. White, S. Ravichandran, P. Kumar, K. Talsania, V. Chen, A. Ghebremedhin, B. Karanam, A. Bin Salam, R. Amin, T. Odzorig, T. Aiken, V. Nguyen, Y. Bian, J. C. Zarif, A. E. de Groot, M. Mehta, L. Fan, X. Hu, A. Simeonov, N. Pate, M. Abu-Asab, M. Ferrer, N. Southall, C. Y. Ock, Y. Zhao, H. Lopez, S. Kozlov, N. de Val, C. C. Yates, B. Baljinnyam, J. Marugan and U. Rudloff, *Sci. Transl. Med.*, 2020, **12**, eaax6337.

19 D. Zhu, C. Hu, F. Fan, Y. Qin, C. Huang, Z. Zhang, L. Lu, H. Wang, H. Sun, X. Leng, C. Wang, D. Kong and L. Zhang, *Biomaterials*, 2019, **206**, 25–40.

20 R. Lu, C. Groer, P. A. Kleindl, K. R. Moulder, A. Huang, J. R. Hunt, S. Cai, D. J. Aires, C. Berkland and M. L. Forrest, *J. Controlled Release*, 2019, **306**, 165–176.

21 S. Bhagchandani, J. A. Johnson and D. J. Irvine, *Adv. Drug Delivery Rev.*, 2021, **175**, 113803.

22 L. Gu, X. Kong, M. Li, R. Chen, K. Xu, G. Li, Y. Qin and L. Wu, *Chem. Commun.*, 2024, **60**, 5474–5485.

23 H. O. Kim, E. Kim, Y. An, J. Choi, E. Jang, E. B. Choi, A. Kukreja, M. H. Kim, B. Kang, D. J. Kim, J. S. Suh, Y. M. Huh and S. Haam, *Macromol. Biosci.*, 2013, **13**, 745–754.

24 C. Park, J.-W. Lim, G. Park, H.-O. Kim, S. Lee, Y. H. Kwon, S.-E. Kim, M. Yeom, W. Na, D. Song, E. Kim and S. Haam, *J. Mater. Chem. B*, 2021, **9**, 9658–9669.

25 J. H. Lam, A. K. Khan, T. A. Cornell, T. W. Chia, R. J. Dress, W. W. W. Yeow, N. K. Mohd-Ismail, S. Venkataraman, K. T. Ng, Y. J. Tan, D. E. Anderson, F. Ginhoux and M. Nallani, *ACS Nano*, 2021, **15**, 15754–15770.

26 S. Kaihara, S. Matsumura, A. G. Mikos and J. P. Fisher, *Nat. Protoc.*, 2007, **2**, 2767–2771.

27 C. Park, E. Kim, G. Park, B. C. Kim, S. Vellampatti, J.-W. Lim, S. Lee, S. Chung, S.-H. Jun, S. Lee, S. Ali, M. Yeom, D. Song and S. Haam, *Adv. Funct. Mater.*, 2023, **33**, 2214603.

28 M. Hematyar, M. Soleimani, A. Es-Haghi and A. Rezaei Mokarram, *Artif. Cells Nanomed. Biotechnol.*, 2018, **46**(sup3), S1226–S1235.

29 M. Sauter, R. J. Sauter, H. Nording, M. Olbrich, F. Emschermann and H. F. Langer, *Star Protoc.*, 2022, **3**, 101664.

30 E. Girard, G. Chagnon, A. Moreau-Gaudry, C. Letoublon, D. Favier, S. Dejean, B. Trilling and B. Nottelet, *J. Biomed. Mater. Res. B Appl. Biomater*, 2021, **109**, 410–419.

31 P. Kubisa, G. Lapienis and T. Biela, *Polym. Adv. Technol.*, 2021, **32**, 3857–3866.

32 Y. Cai, X. Zu, Q. Shuai, F. Zhu, J. Xu, X. Gao and X. Sun, *Biomater. Sci.*, 2020, **8**, 2274–2282.

33 X. Zhang, J. C. M. van Hest and Y. Men, *ACS Appl. Nano Mater.*, 2024, **7**, 14865–14888.

34 J. Chen, H. Fang, Y. Hu, J. Wu, S. Zhang, Y. Feng, L. Lin, H. Tian and X. Chen, *Bioact. Mater.*, 2022, **7**, 167–180.

35 Y. Pan, Y. Qi, X. Li, S. Luan and Y. Huang, *Adv. Funct. Mater.*, 2021, **31**, 2105742.

36 A. C. Vieira, L. L. Chaves, M. Pinheiro, D. Ferreira, B. Sarmento and S. Reis, *Int. J. Nanomed.*, 2016, **11**, 2601–2617.

37 N. Aibani, T. N. Khan and B. Callan, *Int. J. Pharm.: X*, 2020, **2**, 100040.

38 Q. Li, X. Li and C. Zhao, *Front. Bioeng. Biotechnol.*, 2020, **8**, 437.

39 J. Kang, A. Tahir, H. Wang and J. Chang, *Wiley Interdiscip. Rev.: Nanomed. Nanobiotechnol.*, 2021, **13**, e1700.

40 Y. Hou, R. Liu, X. Hong, Y. Zhang, S. Bai, X. Luo, Y. Zhang, T. Gong, Z. Zhang and X. Sun, *J. Controlled Release*, 2021, **333**, 162–175.

41 B. S. Ou, O. M. Saouaf, J. Baillet and E. A. Appel, *Adv. Drug Delivery Rev.*, 2022, **187**, 114401.

42 S. M. Kaech, E. J. Wherry and R. Ahmed, *Nat. Rev. Immunol.*, 2002, **2**, 251–262.